

# Impact of flavor changing processes on prospects for majoron discovery at intensity-frontier searches

---

Krzysztof Jodłowski,<sup>a,b,c</sup> Chih-Ting Lu<sup>a,b</sup>

<sup>a</sup>*Department of Physics and Institute of Theoretical Physics Nanjing Normal University, Nanjing, 210023, China*

<sup>b</sup>*5 Nanjing Key Laboratory of Particle Physics and Astrophysics, Nanjing, 210023, China*

<sup>c</sup>*Particle Theory and Cosmology Group, Center for Theoretical Physics of the Universe, Institute for Basic Science (IBS), Daejeon 34126, Korea*

*E-mail:* [kjodlowski@njnu.edu.cn](mailto:kjodlowski@njnu.edu.cn), [ctl@njnu.edu.cn](mailto:ctl@njnu.edu.cn)

**ABSTRACT:** The singlet majoron  $J$  is the pseudo–Nambu–Goldstone boson of a global, anomaly-free  $U(1)_{B-L}$  symmetry whose spontaneous breaking generates Majorana masses for right-handed neutrinos. At tree level, the only direct coupling of  $J$  to Standard Model fields is  $J\nu\nu \propto m_\nu/f$  (where  $m_\nu$  denotes the light neutrino mass and  $f$  the  $B-L$  breaking scale). Couplings to charged fermions and gauge bosons, in contrast, arise only at loop level. Consequently,  $J$  can be long-lived over wide regions of parameter space, motivating displaced-decay searches. We study majoron production and displaced decays at proton beam dump experiments, neutrino facilities, and LHC forward detectors (including DUNE, NA62, FASER/FASER2, MATHUSLA, and SHiP), and we quantify the resulting reach in the  $(m_J, f)$  plane. We show that, for realistic seesaw-induced coupling textures, lepton-flavor-violating (LFV)  $\tau$  decays  $\tau \rightarrow \ell J$  ( $\ell = e, \mu$ ) dominate majoron production at these facilities and can extend sensitivity into the intermediate-mass window  $m_J \simeq 0.2\text{--}1.7$  GeV, complementary to supernova bounds at lower masses and to dedicated LFV searches at higher masses. We also identify physically consistent benchmark textures for the matrix  $K = M_D M_D^\dagger / (vf)$  with  $M_D$  denoting the Dirac mass matrix and  $v$  the electroweak scale (including positive semidefinite “anarchical”, single-flavor, and CP-violating cases) and map their impact on experimental reach.

---

## Contents

<b>1</b>	<b>Introduction</b>	<b>1</b>
<b>2</b>	<b>Coupling structure</b>	<b>3</b>
<b>3</b>	<b>Majoron production and decay modes</b>	<b>8</b>
<b>4</b>	<b>Phenomenology: signatures and experimental setup</b>	<b>11</b>
<b>5</b>	<b>Results</b>	<b>12</b>
<b>6</b>	<b>Conclusions</b>	<b>17</b>

---

## 1 Introduction

The observation of neutrino oscillations has established that at least two neutrinos are massive and that lepton flavors mix, providing unambiguous evidence for physics beyond the Standard Model (SM). Among the most economical and theoretically appealing frameworks to account for these masses is the type-I seesaw mechanism [1–4], in which SM-singlet right-handed neutrinos acquire large Majorana masses, and light neutrino masses arise from the exchange of these heavy states. In many realizations, the seesaw is embedded in a theory with a global, non-anomalous  $U(1)_{B-L}$  symmetry, spontaneously broken by the vacuum expectation value (VEV) of a scalar field. The associated Nambu-Goldstone boson is the *majoron* [5–7]—a pseudoscalar whose phenomenology is intrinsically tied to the structure of the neutrino mass matrix. Unlike generic axion-like particles (ALPs) with arbitrary couplings, the majoron’s interactions are dictated by the seesaw structure, rendering each experimental measurement a direct probe of the neutrino mass generation mechanism.

We consider the singlet-majoron type-I seesaw extension of the SM, augmented by a complex scalar singlet  $S$  carrying  $B-L$  charge  $+2$  (so that its VEV generates RHN Majorana masses):

$$\mathcal{L} \supset -y_{\alpha i} \bar{L}_\alpha \tilde{H} N_i - \frac{1}{2} \lambda_{ij} S \bar{N}_i^c N_j + \text{h.c.} - V(H, S), \quad (1.1)$$

where  $L_\alpha$  ( $\alpha = e, \mu, \tau$ ) denote the SM lepton doublets,  $\tilde{H} = i\sigma_2 H^*$  is the conjugate Higgs doublet,  $N_i$  ( $i = 1, 2, 3$ ) are SM-singlet right-handed neutrinos (RHNs),<sup>1</sup>  $y_{\alpha i}$  are the neutrino Yukawa couplings, and  $\lambda_{ij} = \lambda_{ji}$  parameterize the Majorana Yukawa interactions. The scalar potential  $V(H, S)$  respects the global  $U(1)_{B-L}$  symmetry under which leptons

---

<sup>1</sup>While introducing only two RHNs is also possible, we focus on the SM extended by three RHNs; see the discussion in Sec. 2.

transform with charge  $-1$ :  $L_\alpha \rightarrow e^{-i\theta} L_\alpha$ ,  $N_i \rightarrow e^{-i\theta} N_i$ , and  $S \rightarrow e^{+2i\theta} S$  (while quarks transform with charge  $+1/3$ ).

Spontaneous symmetry breaking occurs when both scalars acquire VEVs,

$$\langle H \rangle = \frac{1}{\sqrt{2}} \begin{pmatrix} 0 \\ v \end{pmatrix}, \quad \langle S \rangle = \frac{f}{\sqrt{2}}, \quad (1.2)$$

with  $v \simeq 246$  GeV the electroweak scale and  $f \gg v$  the  $B-L$  breaking scale. These generate the Dirac and Majorana mass matrices

$$(M_D)_{\alpha i} = \frac{y_{\alpha i} v}{\sqrt{2}}, \quad (M_N)_{ij} = \frac{\lambda_{ij} f}{\sqrt{2}}. \quad (1.3)$$

Integrating out the heavy right-handed neutrinos yields the light neutrino mass matrix via the seesaw formula,

$$m_\nu = -M_D M_N^{-1} M_D^T, \quad (1.4)$$

which naturally explains the smallness of neutrino masses for  $f \sim 10^7\text{--}10^{15}$  GeV.

The complex scalar  $S$  can be parameterized as

$$S(x) = \frac{1}{\sqrt{2}}(f + \rho(x)) \exp \left[ i \frac{J(x)}{f} \right], \quad (1.5)$$

where  $\rho(x)$  is the massive radial mode and  $J(x)$  is the massless Nambu–Goldstone boson associated with the spontaneous breaking of  $U(1)_{B-L}$ —the majoron. The radial mode  $\rho$  acquires a mass  $m_\rho \simeq \sqrt{2\lambda_S} f$ , where  $\lambda_S$  is the quartic self-coupling of  $S$  in  $V(H, S)$ , and it decouples from the low-energy phenomenology, whereas the majoron remains in the spectrum as a light degree of freedom with derivative couplings suppressed by  $1/f$ .

In the exact  $U(1)_{B-L}$  limit, the majoron is strictly massless and couples derivatively to the lepton-number current. However, exact continuous global symmetries are not expected to survive in a UV-complete theory of quantum gravity [8–10]. Planck-suppressed operators and possibly nonperturbative gravitational effects, such as Euclidean wormholes, explicitly break  $U(1)_{B-L}$  [11–13], lifting the flat direction of the scalar potential. Additional sources of explicit breaking include higher-dimensional operators suppressed by a UV cutoff. These effects generically induce a mass  $m_J \neq 0$ , promoting the majoron to a pseudo-Nambu-Goldstone boson. The resulting low-energy effective Lagrangian for the majoron field takes the form

$$\mathcal{L}_J = \frac{1}{2} \partial_\mu J \partial^\mu J - \frac{1}{2} m_J^2 J^2 + \mathcal{L}_{\text{int}}, \quad (1.6)$$

where  $m_J$  parameterizes the explicit breaking strength. Throughout this work, we treat  $m_J$  as a free parameter. We assume that in the parameter space of interest explicit  $U(1)_{B-L}$  breaking primarily manifests itself as the mass term  $m_J$ , while additional shift-symmetry-violating operators affecting  $J$  couplings are negligible.

A majoron with mass in the MeV–GeV range has received considerable recent attention [14, 15], with studies demonstrating its potential impact on Big Bang Nucleosynthesis through modifications to primordial light-element abundances [14]. However, the

updated BBN bound on majoron is weak,  $1/f \simeq g/m_\nu \sim 0.2/\text{GeV}$  [16]. Astrophysical constraints—particularly from supernovae—are stringent [17–22] but are typically restricted to  $m_J \lesssim \mathcal{O}(0.1 \text{ GeV})$  in the simplest production and decay regimes; above this threshold, constraints weaken appreciably, though bounds from secondary neutrino fluxes remain non-negligible [19]. For  $m_J \gtrsim 1 \text{ GeV}$ ,  $B$ -meson factories and dedicated lepton-flavor-violating (LFV) searches provide complementary coverage [23–27]. The intermediate window  $0.1 \text{ GeV} \lesssim m_J \lesssim 1 \text{ GeV}$  remains comparatively underexplored: supernova bounds lose sensitivity once the majoron mass exceeds the core temperature, while rare  $B$  decays provide complementary coverage at higher masses, though the reach depends strongly on whether  $J$  decays visibly into photons, hadrons, leptons or escapes the detector. Recent reanalyses of intensity-frontier (IF) data indicate important but incomplete coverage in this window [24], motivating dedicated searches exploiting alternative production mechanisms.

In this work, we study the singlet majoron [5] in intensity-frontier experiments, focusing on the intermediate-mass regime  $m_J \lesssim m_\tau$ . We demonstrate that LFV decays,  $\tau \rightarrow \ell J$  and/or  $\mu \rightarrow e J$ , provide the leading majoron production channels in this window, and we assess the resulting sensitivity at beam dump experiments, neutrino facilities, and forward detectors at the LHC [23, 24, 28].

Our emphasis is on a systematic assessment of their experimental impact across physically consistent  $K$ -matrix textures, including anarchic benchmarks satisfying positivity constraints, single-flavor textures, and CP-violating benchmarks motivated by leptogenesis.

## 2 Coupling structure

In the following, we provide the full form of the interaction Lagrangian. As the Nambu-Goldstone boson of a global  $U(1)_{B-L}$ ,  $J$  couples derivatively to the  $B-L$  current. We consider global  $U(1)_{B-L}$  that could be promoted to a gauge symmetry without anomalies in the SM supplemented with three RHNs. A recent work [29] argues that if a single VEV breaks several global  $U(1)$  combinations—some gauge-anomalous (e.g.  $L$ ) and one gauge-anomaly free ( $B-L$ )—the resulting Nambu-Goldstone boson necessarily aligns with the anomaly-free  $B-L$ , further justifying our choice. Whenever we use results derived in lepton-number majoron notation in the literature, we match onto the same low-energy effective couplings relevant for on-shell  $J$  processes considered here [23, 30].

Since the charged-lepton Dirac masses preserve  $U(1)_{B-L}$ , one can choose a basis in which the majoron field is removed from the charged-fermion mass/Yukawa terms by  $U(1)_{B-L}$ -preserving field redefinitions. Equivalently, any apparent tree-level  $J$ -coupling to charged SM fermions is a derivative coupling to a conserved current and does not lead to physical on-shell amplitudes. Physical couplings of  $J$  to charged fermions arise only radiatively once EW symmetry is broken and the seesaw sector is integrated out. Upon using the equations of motion, the only irreducible tree-level coupling to SM fields is  $J\nu\nu$ , which is proportional to the Majorana neutrino masses, and therefore is negligible for our purposes. Similarly, couplings involving  $J$  and heavy neutrinos do not affect majoron production or decay modes at intensity-frontier.

For ease of comparison, we adopt the conventions of Ref. [31], while indicating the explicit matching to Ref. [32]. The tree-level coupling between the majoron and active neutrinos reads

$$\mathcal{L}_{\text{int}}^{\text{tree}} = -\frac{\partial_\mu J}{4f} \sum_{i=1}^3 \bar{\nu}_i \gamma^\mu \gamma_5 \nu_i = \frac{iJ}{2f} \sum_{i=1}^3 m_i \bar{\nu}_i \gamma_5 \nu_i, \quad (2.1)$$

where  $f$  denotes the symmetry-breaking scale and the second equality follows from the equations of motion. These couplings are phenomenologically negligible, being suppressed by  $m_\nu/f \lesssim \mathcal{O}(10^{-17})$ .

Radiative corrections at one [33, 34] and two loops [32] induce interactions with charged fermions  $\psi$  and gauge bosons

$$\begin{aligned} \mathcal{L}_{\text{int}}^{\text{loop}} = & \frac{1}{2f} \partial_\mu J \bar{\psi} \gamma^\mu (C_V + C_A \gamma_5) \psi + \frac{g_{J\gamma\gamma}}{4} J F_{\mu\nu} \tilde{F}^{\mu\nu} + \frac{g_{J\gamma Z}}{2} J F_{\mu\nu} \tilde{Z}^{\mu\nu} \\ & + \frac{g_{Jgg}}{4} J G_{\mu\nu}^a \tilde{G}^{a\mu\nu} + \frac{g_{JZZ}}{4} J Z_{\mu\nu} \tilde{Z}^{\mu\nu} + \frac{g_{JWW}}{4} J W_{\mu\nu}^+ \tilde{W}^{-\mu\nu}. \end{aligned} \quad (2.2)$$

Here,  $\tilde{V}^{\mu\nu} \equiv \frac{1}{2} \epsilon^{\mu\nu\rho\sigma} V_{\rho\sigma}$  denotes a field-strength tensor dual to  $V^{\mu\nu}$ .<sup>2</sup> Additional operators coupling  $J$  to  $\gamma H$ ,  $ZH$  (with  $H$  the SM Higgs), or inducing flavor-violating quark currents are either seesaw-suppressed or arise at two-loop order, rendering their phenomenological impact negligible.

The key role in majoron phenomenology is played by the dimensionless matrix  $K$ , which has the following form:

$$K \equiv \frac{M_D M_D^\dagger}{v f} = \begin{pmatrix} K_{ee} & K_{e\mu} & K_{e\tau} \\ K_{e\mu}^* & K_{\mu\mu} & K_{\mu\tau} \\ K_{e\tau}^* & K_{\mu\tau}^* & K_{\tau\tau} \end{pmatrix}, \quad (2.3)$$

where  $M_D$  is the Dirac mass term that mixes the active neutrinos with the sterile neutrinos,  $v$  is the Higgs VEV; the diagonal entries are real, while the off-diagonal ones can be complex. The matrix  $K$  has several important properties: it enters the expressions for the majoron couplings generated at loop level [5, 33], being constructed from  $M_D M_D^\dagger$ , it is hermitian and positive semidefinite by construction,<sup>3</sup> even when one light neutrino is massless [35]. Crucially, while neutrino oscillation data probe the combination  $M_D M_N^{-1} M_D^T$  (cf. Eq. (1.4)), majoron couplings depend on  $M_D M_D^\dagger$ , providing complementary access to the seesaw parameter space [33].

The couplings to gauge bosons in Eq. (2.2) are generated by the SM particles in one- and two-loop diagrams—we follow the comprehensive discussion of Ref. [32]. Each of these contributions is proportional to  $h(m_J^2/(4m_{\text{SM}}^2))$ , where the loop function  $h(x)$  is defined by

$$h(x) = -\frac{1}{4x} \left( \log[1 - 2x + 2\sqrt{x(x-1)}] \right)^2 - 1. \quad (2.4)$$

<sup>2</sup>The photon and gluon operators are proportional to  $\partial^2 J V \tilde{V}$  and vanish for massless majoron [32]. Application of the equations of motion yields Eq. (2.2). Therefore, for processes in which  $J$  appears exclusively as an on-shell external state—as is the case throughout this work—the two forms are equivalent.

<sup>3</sup>It is positive definite if  $M_D$  has full rank—this is generic in the three-RHN setup. While special textures could reduce the rank, we study positive definite  $K$  only.

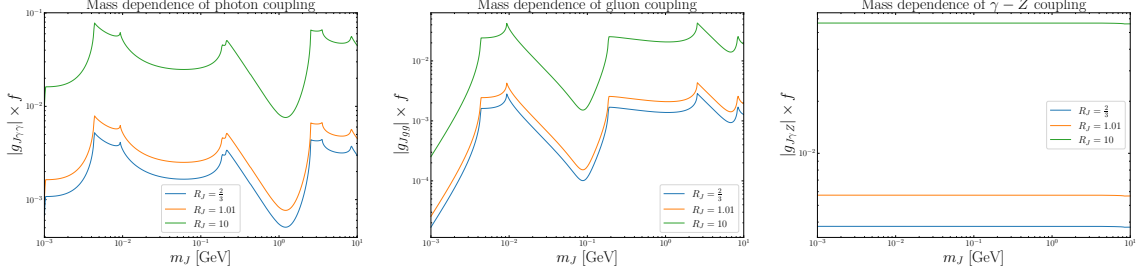


**Figure 1.** Functional dependence of the majoron couplings to gauge bosons, which affect the decay widths and production modes of the majoron. We show three examples (indicated by blue, orange, and green lines) of the “anarchical” benchmark defined by Eq. (2.14). A similar dependence holds for the other benchmarks, in particular those given by Eq. (2.17) and Eq. (2.19).

Its asymptotic forms are

$$h(x) \simeq \frac{x}{3} + \mathcal{O}(x^2) \quad (x \rightarrow 0) \quad \text{and} \quad h(x) \simeq -1 \quad (x \rightarrow \infty). \quad (2.5)$$

As a result,  $|h(x)|$  is suppressed for small  $x$ , achieves its maximum at  $x = 1$ , and rapidly approaches its asymptotic value  $h(x) \rightarrow -1$  for  $x \rightarrow \infty$ . This behavior explains the peak and trough structure of the mass dependence of gauge boson couplings shown in Fig. 1.

For qualitative estimates relevant to the phenomenology of the sub-GeV majoron, one needs the functional dependence of the gauge boson couplings in the  $m_J \rightarrow 0$  limit. Given the behavior of the  $h(x)$  function, the lightest SM particle in the loop provides the dominant contribution to the coupling, resulting in

$$g_{Jgg} \simeq \frac{\alpha_S m_J^2}{384\pi^3 m_u^2 v} \text{Tr}(K), \quad (2.6)$$

$$g_{J\gamma\gamma} \simeq \frac{\alpha m_J^2}{96\pi^3 v} \left[ \left( \frac{K_{ee}}{m_e^2} + \frac{K_{\mu\mu}}{m_\mu^2} + \frac{K_{\tau\tau}}{m_\tau^2} \right) - \frac{\text{Tr} K}{2m_e^2} \right], \quad (2.7)$$

$$g_{JZ\gamma} \simeq -\frac{\alpha}{8\pi^3 v} \text{Tr} K. \quad (2.8)$$

Note that among the phenomenologically-relevant majoron couplings to gauge bosons, only  $g_{JZ\gamma}$  does not vanish in the  $m_J \rightarrow 0$  limit because the  $Z$  boson is massive. Therefore, it dominates over the two-photon coupling in this regime,  $\frac{g_{JZ\gamma}}{g_{J\gamma\gamma}} \xrightarrow{m_J \rightarrow 0} \infty$ .

Let us discuss the fermion sector, which will play a key phenomenological role in the production and decays of the majoron. Specializing Eq. (2.2) in the fermion sector—leptons and quarks—one obtains

$$\begin{aligned} \mathcal{L}_{\text{int.}} \supset & \frac{1}{2f} \partial_\mu J (\bar{e} \bar{\mu} \bar{\tau}) \gamma^\mu \left( C_V^\ell + C_A^\ell \gamma_5 \right) \begin{pmatrix} e \\ \mu \\ \tau \end{pmatrix} \\ & + \frac{1}{2f} \partial_\mu J (\bar{u} \bar{c} \bar{t}) \gamma^\mu \left( C_V^u + C_A^u \gamma_5 \right) \begin{pmatrix} u \\ c \\ t \end{pmatrix} + \frac{1}{2f} \partial_\mu J (\bar{d} \bar{s} \bar{b}) \gamma^\mu \left( C_V^d + C_A^d \gamma_5 \right) \begin{pmatrix} d \\ s \\ b \end{pmatrix}. \end{aligned} \quad (2.9)$$

Then, matching Eq. (2.9) to Eqs. 10 and 11 of Ref. [32], one obtains for leptons [24]

$$C_V^\ell = \frac{f K}{8\pi^2 v}, \quad C_A^\ell = -\frac{f}{8\pi^2 v} \left( K - \frac{\text{Tr}(K)}{2} \mathbb{1}_{3 \times 3} \right), \quad (2.10)$$

where the relation for off-diagonal elements,  $C_V^o = -C_A^o$ , originates from the purely left-handed nature of weak interaction. The trace term affects only diagonal axial couplings.

For quarks, we obtain

$$C_V^u = C_V^d = 0, \quad C_A^u = -C_A^d = \frac{f}{16\pi^2 v} \text{Tr}(K) \mathbb{1}_{3 \times 3}. \quad (2.11)$$

While both  $C^\ell$  and  $C^{u/d}$  are parametrically similar, due to their origin from the same order in perturbation theory, there are no flavor-violating (FV) quark couplings at 1-loop, and the two-loop result is additionally suppressed ( $\sim 1/(16\pi^2)$ ). On the other hand, the values of the off-diagonal leptonic couplings,  $C_V^{l_i l_j}$ ,  $C_A^{l_i l_j}$  for  $i \neq j$ , can be comparable to the flavor-conserving ones and dominate particular observables when the relevant diagonal entries are small or cancellations occur. As a result, flavor-violating decays of heavy leptons, taus in particular, can be an efficient production mechanism of  $J$ .

To obtain Eq. (2.10) and Eq. (2.11), we used the equations of motion, where for quarks, one needs to take into account the quark axial-current identity

$$\partial_\mu (\bar{q} \gamma^\mu \gamma_5 q) = 2im_q \bar{q} \gamma_5 q + \text{anomaly}, \quad (2.12)$$

where the anomaly terms are consistently taken into account when deriving the effective coupling to  $G\tilde{G}$ , as discussed in Ref. [32]. Moreover, for light quarks, the anomaly terms must be combined with non-perturbative chiral physics when matching below  $\Lambda_{\text{QCD}}$ .

Since the low-energy effective couplings in Eq. Eq. (2.2) are not  $SU(2)_L$  invariant after electroweak symmetry breaking, the majoron can also be produced in helicity-suppressed decays of light pseudoscalars, such as pions and kaons [36]. However, these are restricted to lower masses,  $m_J \lesssim 100 \text{ MeV}$ , and do not lead to competitive limits compared to astrophysical probes or limits derived from  $\tau$  decays [37, 38].

The majoron coupling to nucleons is obtained by matching quark-level axial/pseudoscalar operators to nucleon matrix elements using the axial Ward identity (including the anomaly) together with nucleon axial charges  $\Delta_q^N$ . We follow the standard treatment used in Ref. [32] and evaluate the resulting effective  $J\bar{N}i\gamma_5 N$  coupling using lattice inputs for  $\Delta_q^N$ . Using  $\Delta_u^p = 0.847(37)$ ,  $\Delta_d^p = -0.407(24)$ ,  $\Delta_s^p = -0.035(9)$  from Refs. [39, 40] and isospin symmetry, we obtain

$$\mathcal{L}_{JNN} = \frac{i J \text{tr}(K)}{16\pi^2 v} [-1.29(3) m_p \bar{p} \gamma_5 p + 1.22(3) m_n \bar{n} \gamma_5 n], \quad (2.13)$$

representing a percent-level correction to the result of Ref. [32].

**Benchmarks:** In this work, we study several representative benchmarks of the singlet majoron model. In particular, we consider the bottom-up phenomenological parameterization of Ref. [31], which we call the ‘‘anarchical’’ benchmark, in which  $K$  has degenerate

diagonal entries  $K^d$  and degenerate off-diagonal entries  $K^o$ , parameterized by the ratio  $R_J = |K^d/K^o|$ ,

$$K_{\text{anarch}} = \begin{pmatrix} K^d & K^o & K^o \\ K^o & K^d & K^o \\ K^o & K^o & K^d \end{pmatrix} = \frac{8\pi^2 v}{f} \begin{pmatrix} R_J & 1 & 1 \\ 1 & R_J & 1 \\ 1 & 1 & R_J \end{pmatrix}. \quad (2.14)$$

Its eigenvalues are positive if and only if  $K^d - K^o > 0$  and  $K^d + 2K^o > 0$ . For positive real  $K^o$ , this requires  $R_J > 1$ ; for negative real  $K^o$ , one needs  $R_J > 2$ . Similar considerations apply to the matrix

$$\begin{pmatrix} K^d & \pm K^o & \pm K^o \\ \pm K^o & K^d & \pm K^o \\ \pm K^o & \pm K^o & K^d \end{pmatrix}, \quad (2.15)$$

for any choice of the signs as long as the resulting matrix is hermitian. Note that with the ansatz given by Eq. (2.14), the couplings to matter fields are as follows (see Eq. (2.2)):

$$\begin{aligned} (C_V^\ell)^d &= 2(C_A^\ell)^d = R_J, & (C_V^\ell)^o &= -(C_A^\ell)^o = 1, \\ C_V^u &= C_V^d = (C_A^u)^o = (C_A^d)^o = 0, & (C_A^u)^d &= -(C_A^d)^d = \frac{3}{2}R_J. \end{aligned} \quad (2.16)$$

Ref. [31] considered  $R_J = 2/3$  and  $R_J = 10$ —only the *latter* benchmark leads to positive-definite  $K$ . For completeness, we show results for three such benchmarks:  $R_J = 2/3$ ,  $R_J = 1.01$ , and  $R_J = 10$ . The last one corresponds either to a larger number of sterile neutrinos or to a small negative value of  $K^o$ , while  $R_J = 1.01$  plays the role of saturating the positive-definiteness bound and corresponds to maximal mixing.

In addition, we consider single-flavor textures,

$$K_{e\tau} = K^d \begin{pmatrix} 1 & 0 & \kappa_{e\tau} \\ 0 & 1 & 0 \\ \kappa_{e\tau}^* & 0 & 1 \end{pmatrix}, \quad K_{\mu\tau} = K^d \begin{pmatrix} 1 & 0 & 0 \\ 0 & 1 & \kappa_{\mu\tau} \\ 0 & \kappa_{\mu\tau}^* & 1 \end{pmatrix}, \quad (2.17)$$

with  $|K^d| = 8\pi^2 v/f$ , and where the  $\kappa_{\alpha\beta}$  parameters are bounded by the requirement of positive-definiteness of the  $K$  matrix:  $|\kappa_{\alpha\beta}| < 1$ . We study cases  $\kappa_{\tau\mu} = 0.01$  and  $\kappa_{\tau\mu} = 0.5$ , which correspond to hierarchical and anarchical regimes between the diagonal and off-diagonal elements, respectively. The couplings to SM fermions read as follows for  $K_{e\tau}$ , with analogous expressions holding for  $K_{\mu\tau}$  and for the  $K^{\text{CPV}}$  benchmarks:

$$\begin{aligned} (C_V^\ell)^d &= 2(C_A^\ell)^d = 1, & (C_V^\ell)^{e\tau} &= -(C_A^\ell)^{e\tau} = \kappa_{e\tau}, \\ C_V^u &= C_V^d = (C_A^u)^o = (C_A^d)^o = 0, & (C_A^u)^d &= -(C_A^d)^d = \frac{3}{2}. \end{aligned} \quad (2.18)$$

Finally, we consider benchmarks with a maximally CP-violating parameterization that is motivated by leptogenesis,

$$K^{\text{CPV}} = K^d \begin{pmatrix} 1 & i\kappa & i\kappa \\ -i\kappa & 1 & i\kappa \\ -i\kappa & -i\kappa & 1 \end{pmatrix}, \quad (2.19)$$

where  $\kappa < 1/\sqrt{3}$  is a positive real parameter, as required by positive-definiteness of  $K^{\text{CPV}}$ . Similarly to the single-flavor textures, we study cases  $\kappa = 0.01$  and  $\kappa = 0.577$ ; the latter is chosen to nearly saturate the positive-definiteness bound  $\kappa < 1/\sqrt{3} \approx 0.5774$ , analogously to the role played by  $R_J = 1.01$  in the anarchical benchmark. The SM-fermion coupling structure is analogous to the one given by Eq. (2.18).

### 3 Majoron production and decay modes

**$J$  production modes:** The leading majoron production mode is LFV  $\tau$  decay,  $\tau \rightarrow \mu J$  and  $\tau \rightarrow e J$ .

The decay widths for flavor-violating decays of a fermion  $\psi_i$  into  $\psi_j$  and  $J$  are given by [28]

$$\begin{aligned} \Gamma(\psi_i \rightarrow \psi_j J) &= \frac{m_i^3}{64\pi f^2} \sqrt{(1-r_J^2)^2 + r_J^4 - 2r_J^2(1+r_J^2)} \\ &\quad \times \left[ \left( (C_A^{ij})^2 + (C_V^{ij})^2 \right) (1-r_J^2)^2 - \left( (C_V^{ij})^2 (1-r_J)^2 + (C_A^{ij})^2 (1+r_J)^2 \right) r_J^2 \right] \\ &\simeq \frac{m_i^3}{64\pi f^2} \left( (C_A^{ij})^2 + (C_V^{ij})^2 \right), \end{aligned} \quad (3.1)$$

where  $r_{j,J} = m_{j,J}/m_i$  and the last relation holds for  $m_{j,J} \ll m_i$ .

Subdominant production modes that do not improve the sensitivity for any benchmark are three-body meson decays, three- or four-body lepton decays, and proton bremsstrahlung [31, 37]. We verified that these channels yield negligible event rates for all the benchmarks considered and do not discuss them further.

The  $\tau$  spectrum is generated by leptonic decays of forward-produced charm mesons, dominantly  $D_s^\pm \rightarrow \tau^\pm \nu_\tau$  and, subleading,  $D^\pm \rightarrow \tau^\pm \nu_\tau$ . We simulated forward charm production with PYTHIA 8 using the Monash tune [41, 42] by using `SoftQCD:all` and disabling `HardQCD` to avoid double counting. For the LHC  $\tau$  spectrum we also used the dedicated Monte Carlo generator SIBYLL [43], finding consistent results to the ones obtained by using PYTHIA 8. In the simulation, we decay  $D_s^\pm$  and  $D^\pm$  to  $\tau^\pm$  and weight each event by the corresponding branching fraction. Since the SM leptonic rate is helicity-suppressed,

$$\text{BR}(D_s \rightarrow \ell \nu_\ell) = \frac{G_F^2}{8\pi} \tau_{D_s} f_{D_s}^2 |V_{cs}|^2 m_{D_s} m_\ell^2 \left( 1 - \frac{m_\ell^2}{m_{D_s}^2} \right)^2, \quad (3.2)$$

implying  $\text{BR}(D_s \rightarrow \mu \nu)/\text{BR}(D_s \rightarrow \tau \nu) \simeq 0.10$  and a negligible electron mode.

**$J$  decays:** We discuss the available decays of the majoron originating from its couplings given by Eq. (2.2) and Eq. (2.9).

For  $m_J < 2m_e$ , the only available decay states are: a pair of photons, a pair of active neutrinos, and  $\gamma \nu \nu$ . However, only the first of these channels is phenomenologically relevant, since the last two are suppressed by the active neutrino masses or by the Fermi constant and phase-space suppression, respectively; as a result, they do not play a role in

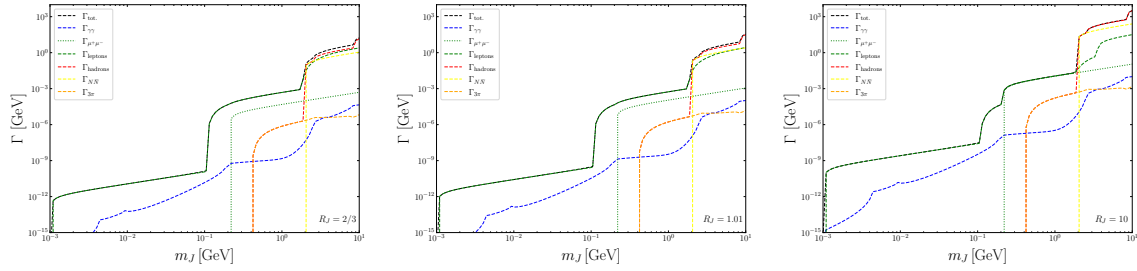


**Figure 2.** Majoron partial decay widths for  $K = K_{\text{anarch}}$  benchmarks:  $R_J = 2/3$  (left),  $R_J = 1.01$  (center), and  $R_J = 10$  (right). We fixed  $f = 1$  GeV, while the general case is obtained by rescaling by  $(1 \text{ GeV}/f)^2$ .

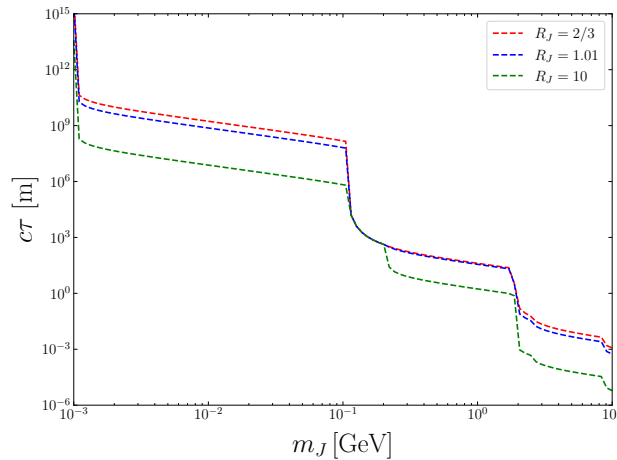


**Figure 3.** Majoron proper decay length  $c\tau$  for the anarchical benchmarks:  $R_J = 2/3$  (red),  $R_J = 1.01$  (blue), and  $R_J = 10$  (green). We fixed  $f = 10^7$  GeV, which corresponds to a typical value that can be probed at IF, see Sec. 5. The general case is obtained by rescaling by  $(f/10^7 \text{ GeV})^2$ .

our analysis. On the other hand, the majoron-photons coupling can be sizeable, and leads to the well-known decay width

$$\Gamma(J \rightarrow \gamma\gamma) = \frac{g_{J\gamma\gamma}^2 m_J^3}{64\pi}. \quad (3.3)$$

Above the electron pair threshold, the majoron can decay into SM fermions. The flavor-conserving decays widths are given by [28]

$$\Gamma(J \rightarrow \psi_i \bar{\psi}_i) = \frac{m_i^2 m_J}{8\pi f^2} (C_A^{ii})^2 \sqrt{1 - \frac{4m_i^2}{m_J^2}}, \quad (3.4)$$

while the flavor-violating ones are described by

$$\begin{aligned}\Gamma(J \rightarrow \psi_i \bar{\psi}_j + \bar{\psi}_i \psi_j) &= \frac{\sqrt{\left(m_i^2 + m_j^2 - m_J^2\right)^2 - 4m_i^2 m_j^2}}{16\pi f^2 m_J^3} \times \\ &\times \left[ m_J^2 \left( \left(C_A^{ij}\right)^2 (m_i + m_j)^2 + \left(C_V^{ij}\right)^2 (m_i - m_j)^2 \right) - \left( \left(C_A^{ij}\right)^2 + \left(C_V^{ij}\right)^2 \right) (m_i^2 - m_j^2)^2 \right] \\ &\simeq \frac{m_i^2 m_J}{16\pi f^2} \left( \left(C_A^{ij}\right)^2 + \left(C_V^{ij}\right)^2 \right) \left(1 - \frac{m_i^2}{m_J^2}\right)^2, \quad (3.5)\end{aligned}$$

where the approximated relation was obtained in [28] for  $m_j \ll m_i$ . Therefore, for non-zero FV couplings and when kinematically allowed, the charged-lepton final states are  $e^+e^-$ ,  $\mu^\pm e^\mp$ ,  $\mu^+\mu^-$ ,  $e^\pm\tau^\mp$ ,  $\mu^\pm\tau^\mp$ ,  $\tau^-\tau^+$ .

For  $3m_\pi < m_J < 2m_N$ , where  $m_N$  is the nucleon mass, decays into light hadrons become kinematically accessible. Since for the majoron the diagonal axial quark and lepton couplings are of similar strength, see Eq. (2.11), the hadronic decays may become important for  $m_J \simeq 1$  GeV. However, due to the suppression of the gluon coupling and the fact that majoron-quark couplings are smaller than leptonic ones combined with the presence of many open leptonic channels, the hadronic decays are subdominant. We used the public code ALPaca [44] to verify the suppression of the hadronic rates at representative benchmark points for the considered mass range.

For a qualitative understanding of the hadronic decays, the  $J \rightarrow 3\pi$  mode is especially relevant, since it is the leading hadronic mode for an ALP with  $m \lesssim 1$  GeV [45]. For our computational purposes, the leading-order chiral perturbation theory result is sufficient. It reads as follows [45, 46]:

$$\begin{aligned}\Gamma(J \rightarrow \pi^0 \pi^0 \pi^0) &= \frac{\pi m_J m_{\pi^0}^4}{6 f_\pi^2} \left[ \frac{g_{Jgg}}{4 g_s^2} \frac{m_d - m_u}{m_d + m_u} + \frac{C_A^{uu} - C_A^{dd}}{32\pi^2 f} \right]^2 \frac{2}{\left(1 - \frac{m_{\pi^0}^2}{m_J^2}\right)^2} \times \\ &\times \int_{\frac{4m_{\pi^0}^2}{m_J^2}}^{(1 - \frac{m_{\pi^0}}{m_J})^2} dz \sqrt{1 - \frac{4m_{\pi^0}^2}{m_J^2} z} \lambda^{1/2} \left(1, z, \frac{m_{\pi^0}^2}{m_J^2}\right), \quad (3.6)\end{aligned}$$

$$\begin{aligned}\Gamma(J \rightarrow \pi^0 \pi^+ \pi^-) &= \frac{\pi m_J m_{\pi^+}^4}{6 f_\pi^2} \left[ \frac{g_{Jgg}}{4 g_s^2} \frac{m_d - m_u}{m_d + m_u} + \frac{C_A^{uu} - C_A^{dd}}{32\pi^2 f} \right]^2 \frac{12}{\left(1 - \frac{m_{\pi^+}^2}{m_J^2}\right)^2} \times \\ &\times \int_{\frac{4m_{\pi^+}^2}{m_J^2}}^{(1 - \frac{m_{\pi^+}}{m_J})^2} dz \sqrt{1 - \frac{4m_{\pi^+}^2}{m_J^2} z} \left(z - \frac{m_{\pi^+}^2}{m_J^2}\right)^2 \lambda^{1/2} \left(1, z, \frac{m_{\pi^+}^2}{m_J^2}\right), \quad (3.7)\end{aligned}$$

where  $g_s$  is the strong interaction coupling constant and  $\lambda(x, y, z) = x^2 + y^2 + z^2 - 2xy - 2xz - 2yz$  is the Källén function. We numerically implemented Eq. (3.6) and Eq. (3.7), finding that  $J \rightarrow 3\pi$  decays are always subdominant; see Fig. 2.

For  $2m_N < m_J < 2\text{ GeV}$ , decays of  $J$  into a pair of nucleons become relevant. Their decay widths are [32]

$$\Gamma_{J \rightarrow N\bar{N}} = C_{NN}^2 \frac{m_J \sqrt{1 - 4m_N^2/m_J^2}}{8\pi}, \quad (3.8)$$

where

$$C_{p\bar{p}} = \frac{-1.29(3) m_p \text{Tr}(K)}{8\pi^2 v}, \quad C_{n\bar{n}} = \frac{1.22(3) m_n \text{Tr}(K)}{8\pi^2 v}. \quad (3.9)$$

For  $m_J \gg 2\text{ GeV}$ , which lies outside our scope, inclusive hadronic decay widths can be computed using the QCD result invoking quark-hadron duality [46–48],

$$\Gamma(J \rightarrow \text{hadrons}) = 32\pi \alpha_s^2(m_J) m_J^3 \left[ 1 + \left( \frac{97}{4} - \frac{7n_q}{6} \right) \frac{\alpha_s(m_J)}{\pi} \right] \times \left| \frac{g_{Jgg}}{16\pi\alpha_s(m_J)} + \sum_{q=1}^3 \frac{C_{qq}}{32\pi^2 f} \right|^2, \quad (3.10)$$

where  $n_q$  is the number of active quark flavors on scale  $\mu = m_J$ .

#### 4 Phenomenology: signatures and experimental setup

The observable signal consists of high-energy SM particles produced in majoron decays. We consider final states containing either a pair of photons or a pair of charged leptons, including both flavor-conserving and flavor-violating configurations.

The decay probability for these processes within a detector region that extends  $\Delta = L_{\text{max}} - L_{\text{min}}$  is given by

$$p(d) = e^{-L_{\text{min}}/d} - e^{-L_{\text{max}}/d}, \quad (4.1)$$

with  $d = \gamma\beta c\tau$  representing the boosted decay length of the LLP in the laboratory frame, and  $L_{\text{min}}$  denoting the separation between the LLP production vertex and the detector's upstream boundary.

Following LLP production, the expected number of observable events exhibiting the characteristic LLP decay signature within the fiducial volume is

$$N = \int \int dE d\theta \frac{d^2 N}{dE d\theta} p(E, \theta) q_{\text{acc.}}(E, \theta), \quad (4.2)$$

where  $\frac{d^2 N}{dE d\theta}$  represents the differential LLP distribution in energy  $E$  and polar angle  $\theta$  with respect to the beam axis;  $p(E, \theta)$  encodes the decay probability within the detector acceptance, and  $q_{\text{acc.}}(E, \theta)$  captures the geometric and kinematic acceptance after applying selection criteria.

In lepton colliders running at center-of-mass energy equal to the  $Z$  boson mass, the number of events is

$$N = N_Z \times \text{BR}(Z \rightarrow J\gamma) \times p_{J \rightarrow \text{SM}+\text{SM}}(E, \theta), \quad (4.3)$$

where  $N_Z = 2.5 \times 10^{12}$  in the Tera-Z factory [49]. The factor  $\text{BR}(Z \rightarrow J\gamma)$  is obtained from the decay width of the  $Z$  boson into photon and majoron (the secondary production from  $\tau$  decays originating from  $Z \rightarrow \tau\tau$  is subdominant), which reads as follows:

$$\Gamma_{Z \rightarrow J\gamma} = \frac{g_{J\gamma Z}^2 m_Z^3 (1 - m_J^2/m_Z^2)^3}{24\pi}. \quad (4.4)$$

At the  $Z$  pole mass, the SM background to  $e^+e^- \rightarrow \gamma\gamma\gamma$  is negligible [50], however, this decay channel of the majoron,  $J \rightarrow \gamma\gamma$ , is suppressed compared to leptonic decays due to the behavior of the  $g_{J\gamma\gamma}$  coupling. Even under optimistic assumptions about backgrounds, the resulting FCC-ee reach is at best  $1/f \sim 10^{-3}\text{--}10^{-2} \text{ GeV}^{-1}$ . Including leptonic decays leads to a reach of order  $1/f \sim 10^{-4}\text{--}10^{-3} \text{ GeV}^{-1}$ , still well below the sensitivity of beam-dump and LFV searches in the parameter region of interest. Since these limits are not competitive, we omit them from figures 4–6.

At the LHC, the relevant production channels—Drell–Yan, vector-boson fusion, and processes involving sterile neutrinos—do not lead to competitive limits due to the suppressed couplings [51], therefore, we do not discuss them.

**Experiment setup:** In Table 1, we illustrate the experimental landscape—key parameters of the considered detectors together with relevant references. We consider both running (FASER) and proposed (MATHUSLA) LHC far detectors, as well as dedicated past and future beam dump experiments. We investigate two versions of FASER running during the High-Luminosity era of the LHC: an upgraded version of the current FASER detector (called FASER2) and the significantly larger, and requiring new dedicated facility, FPF FASER2 (designed to run at dedicated Forward Physics Facility [52]).

## 5 Results

**Majoron decay widths and lifetime:** In Fig. 2, we present the majoron partial decay widths as a function of  $m_J$  for the three anarchical benchmarks, fixing  $f = 1 \text{ GeV}$  (the general case scales as  $(1 \text{ GeV}/f)^2$ ). The corresponding rest-frame decay length  $c\tau$  is shown in Fig. 3 for  $f = 10^7 \text{ GeV}$ , a representative value probed by intensity-frontier experiments at  $m_J \sim 1 \text{ GeV}$ —see the discussion below.

For  $m_J \lesssim m_\tau - m_e \simeq 1.78 \text{ GeV}$ , the dominant decay modes are in kinematically accessible lepton pairs—both flavor-diagonal ( $e^+e^-$ ,  $\mu^+\mu^-$ ) and flavor-violating ( $\mu^\pm e^\mp$ ). This hierarchy is a direct consequence of the coupling structure of the singlet majoron: the couplings to photons and gluons are proportional to  $m_J^2$  and vanish in the massless-majoron limit (cf. Eq. (2.6)), whereas the one-loop leptonic couplings (Eq. (2.10)) are unsuppressed. Combined with the large multiplicity of open leptonic channels above their respective thresholds, this renders the hadronic ( $J \rightarrow 3\pi$ , computed via Eq. (3.6)–Eq. (3.7)) and diphoton decay modes subdominant throughout the sub- $\tau$  mass range. We verified this conclusion (as well as the decay widths in  $\eta\pi\pi$ ,  $\eta'\pi\pi$ ,  $K\bar{K}$ ) using the public code ALPACA [44] on representative benchmark points, finding consistent results. Above  $m_J \gtrsim 2 \text{ GeV}$ , decays into nucleon pairs and inclusive hadronic final states (Eq. (3.10)) become

Experiment	Energy	Lumi. or $N_{\text{prot.}}$	Transverse size	$L_{\text{min}}$	$\Delta$	Energy cut	Ref.
ArgoNeuT - target	120 GeV	$1.09 \times 10^{20}$	$0.2 \times 0.24 \text{ m}^2$	1033 m	1.3 m	$E > 10 \text{ GeV}$	[24, 53]
ArgoNeuT - hadronic absorber	120 GeV	$1.63 \times 10^{19}$	$0.2 \times 0.24 \text{ m}^2$	318 m	1.3 m	$E > 10 \text{ GeV}$	[24, 53]
BEBC	400 GeV	$2.7 \times 10^{18}$	$3.6 \times 2.5 \text{ m}^2$	404 m	1.85 m	$E > 0.5 \text{ GeV}$	[54, 55]
CHARM	400 GeV	$2.4 \times 10^{18}$	$3 \times 3 \text{ m}^2$	480 m	35 m	$E > 0.5 \text{ GeV}$	[56, 57]
DUNE	120 GeV	$1.1 \times 10^{22}$	$5 \times 5 \text{ m}^2$	574 m	5.88 m	$E > 0.5 \text{ GeV}$	[58]
FASER2	13.6 TeV	$3 \text{ ab}^{-1}$	$r = 1 \text{ m}$	650 m	10 m	$E > 50 \text{ GeV}$	[59, 60]
FPF FASER2	13.6 TeV	$3 \text{ ab}^{-1}$	$r = 1 \text{ m}$	620 m	25 m	$E > 100 \text{ GeV}$	[61, 62]
MATHUSLA	13.6 TeV	$3 \text{ ab}^{-1}$	highly off-axis ( $40 \times 40 \times 11 \text{ m}^3$ )	$\sim 100 \text{ m}$	40 m	$E > 1 \text{ GeV}$	[63, 64]
NA62	400 GeV	$1.0 \times 10^{18}$	$r = 1.13 \text{ m}$	81 m	135 m	$E > 3 \text{ GeV}$	[57]
NuCal	69 GeV	$1.7 \times 10^{18}$	$r = 1.3 \text{ m}$	23 m	64 m	$E > 10 \text{ GeV}$	[57, 65]
SHiP	400 GeV	$6.0 \times 10^{20}$	$2.5 \times 5.5 \text{ m}^2$	33.7 m	50 m	$E > 0.5 \text{ GeV}$	[57]

**Table 1.** Technical specifications and energy thresholds for the detectors considered in this study. For LHC-based experiments, the center-of-mass energy is assumed to be  $\sqrt{s} = 13.6 \text{ TeV}$ . MATHUSLA dimensions (which is a highly off-axis detector covering the high  $p_T$  regime complementary to the forward detectors) follow the updated 40-meter modular design [63].

dominant, but these masses exceed  $m_\tau$  and lie outside the scope of our  $\tau$ -driven production mechanism. The qualitative picture of the majoron branching ratios is similar to the one shown in Fig. 2 also for the single-flavor (Eq. (2.17)) and CP-violating (Eq. (2.19)) benchmarks.

**Majoron production mechanism and the role of LFV:** A key ingredient in our sensitivity projections is that the LFV decays  $\tau \rightarrow \mu J$  and  $\tau \rightarrow e J$ , induced at one loop by the off-diagonal entries of the matrix  $K = M_D M_D^\dagger / (vf)$ , provide the dominant majoron production channel for proton beam dump experiments and forward detectors at the LHC. The copious  $\tau$  flux from  $D_s/D \rightarrow \tau \nu_\tau$  decays in these facilities, combined with the unsuppressed LFV branching fractions (cf. Eq. (2.10)), yields efficient majoron production in the mass window  $200 \text{ MeV} \lesssim m_J \lesssim m_\tau - m_e$ . Subdominant production modes—three-body meson decays, multi-body lepton decays, and proton bremsstrahlung [31, 37]—were checked and found to result in negligible event rates compared to the  $\tau$  LFV channel.

We have also considered majoron production from muon flavor-violating decays  $\mu \rightarrow e J$  at FASER2, exploiting the high-energy ( $E_\mu > 100 \text{ GeV}$ ) muon beam passing through the detector [66] (also see discussion in [67]),

$$N_\mu^{\text{FASER2}} = 4 \times 10^{10}. \quad (5.1)$$

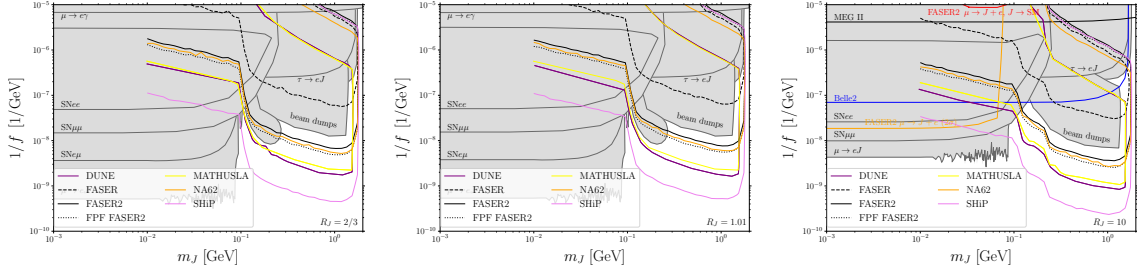


**Figure 4.** Results for the “anarchical” benchmark (see Eq. (2.14)), shown in the  $m_J$  vs.  $1/f$  plane. Sensitivity curves correspond to  $N_{\text{sig}} = 3$  expected displaced-decay events; majorons are produced primarily via  $\tau \rightarrow \ell J$  from forward  $D_s/D \rightarrow \tau\nu_\tau$  decays and are detected through all visible decay channels into charged-lepton pairs (both flavor-conserving and flavor-violating). The gray-shaded region denotes the combined exclusion from past beam-dump experiments (CHARM, BEBC, NuCal). Hatched and shaded regions show existing astrophysical constraints from supernova cooling (SN- $ee$ , SN- $\mu\mu$ , SN- $e\mu$ ) and terrestrial LFV searches ( $\mu \rightarrow e J_{\text{inv.}}$ ,  $\tau \rightarrow \mu J_{\text{inv.}}$ ,  $\tau$  lifetime), as labeled. Colored solid curves show projected reaches for the listed future facilities (see legend); dashed lines indicate projected sensitivities of Belle II and MEG-II. The hierarchy between off-diagonal and diagonal elements is controlled by three values of  $R_J$ :  $R_J = 2/3$  (left),  $R_J = 1.01$  (center), and  $R_J = 10$  (right). In the right panel, we additionally show the reach from  $\mu \rightarrow e J$  production using the high-energy muon flux traversing FASER2 (dotted), as well as limits from excess muon decays  $\mu^\pm \rightarrow J e^\pm$  (orange shading) and from prompt majoron decays following muon decay (red shading); these limits are weaker for the other benchmarks and are omitted there. Note that the  $R_J = 2/3$  benchmark does not yield a positive-semi-definite  $K$  matrix and is shown for comparison only (see text).

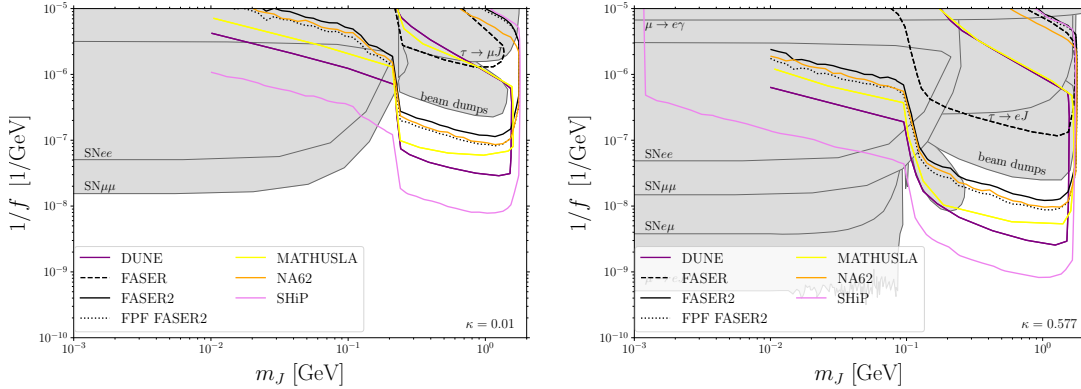


**Figure 5.** Same as Fig. 4, but for the maximally CP-violating texture defined in Eq. (2.19), with  $\kappa = 0.01$  (left) and  $\kappa = 0.577$  (right). The diagonal entries are fixed at  $K^d = 8\pi^2 v/f$ , while  $\kappa$  controls the magnitude of all off-diagonal (purely imaginary) LFV entries and hence the branching fractions  $\text{BR}(\tau \rightarrow \ell J)$ . These benchmarks are motivated by leptogenesis scenarios requiring large CP-violating phases in the seesaw sector.

However, since these probe the same low-mass, low-coupling regime as supernova cooling bounds [20, 68], the astrophysical constraints dominate in all scenarios considered. The results for this channel are shown only for the  $R_J = 10$  benchmark in Fig. 4 (right panel).

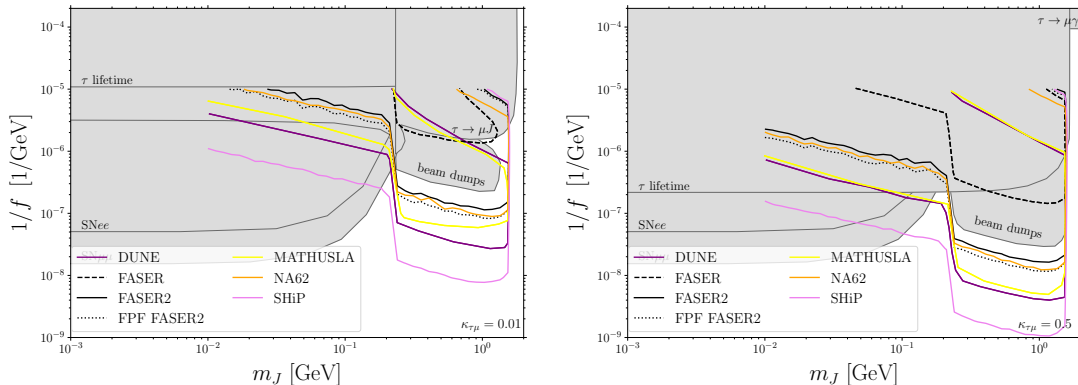


**Figure 6.** Same as Fig. 4, but for the single-flavor  $K_{\mu\tau}$  texture defined in Eq. (2.17), with  $\kappa_{\mu\tau} = 0.01$  (left) and  $\kappa_{\mu\tau} = 0.5$  (right). The diagonal entries are fixed at  $K^d = 8\pi^2 v/f$ , so that  $\kappa_{\mu\tau}$  controls the magnitude of the  $\tau$ - $\mu$  LFV coupling and hence  $\text{BR}(\tau \rightarrow \mu J)$ . The two panels illustrate the transition from a hierarchical regime, in which the off-diagonal entry is suppressed, to a near-anarchical regime with comparable diagonal and off-diagonal couplings.

**Systematic uncertainties:** The dominant source of systematic uncertainty in our projections is the modeling of forward charm meson production ( $D_s^\pm$ ,  $D^\pm$  spectra), which directly affects the  $\tau$  flux and hence the majoron yield. We employed PYTHIA 8 (Monash tune) as our baseline generator and cross-checked with SIBYLL for LHC energies, finding consistent  $\tau$  spectra. Residual uncertainties from the choice of generator, fragmentation model, and forward-production cross section can affect the signal yield by up to a factor of a few; however, owing to the logarithmic scaling of the sensitivity contours with the number of signal events (the approximate scaling is  $(1/f)_{max} \propto \log^{1/2}(N_\tau)$  in the short-lived regime and  $(1/f)_{max} \propto N_\tau^{1/4}$  in the long-lived regime), this translates into a modest shift of the exclusion boundaries in the  $(m_J, 1/f)$  plane. A detailed discussion of these uncertainties can be found in Appendices A and B of Ref. [37] (see also Figures 10 and 11 therein).

**Sensitivity projections:** In Figs. 4–6, we present the projected sensitivity contours in the  $(m_J, 1/f)$  plane for all benchmarks listed in Sec. 2. We include majoron decays into all visible final states (both flavor-diagonal and flavor-violating charged-lepton pairs), which extends the experimental sensitivity also below the dimuon threshold. Since displaced majoron decays into high-energy leptons constitute a background-free signature in all experiments considered, we adopt a signal threshold of  $N_{\text{sig}} = 3$  events.

Among past beam dump experiments, we find that CHARM [56] provides the strongest existing limit, followed by BEBC [54] and NuCal [69]; all three surpass the ArgoNeuT bound [31]. We denote the resulting combined exclusion region as “beam dumps” (gray shading). Among currently operating experiments, NA62 [70] will reach  $f \sim 3 \times 10^8$  GeV for  $m_J \simeq 1$  GeV, while FASER [71], thanks to the higher energy of the LHC beam, extends the sensitivity toward larger masses, up to  $m_J \lesssim m_\tau - m_e$ .

Among future experiments, SHiP provides the single most sensitive projected reach across all benchmarks, probing  $1/f \sim 10^{-6} - 3 \times 10^{-10}$  GeV $^{-1}$  (equivalently  $f$  up to  $\sim 3 \times 10^9$  GeV at  $m_J \simeq 1$  GeV) over the full mass range  $m_J \in [10 \text{ MeV}, 1.77 \text{ GeV}]$ . This

leading sensitivity is driven by SHiP’s combination of high luminosity ( $6 \times 10^{20}$  protons on target during its 15-year run), relatively short baseline ( $L_{\min} = 33.7$  m), and large decay volume ( $\Delta = 50$  m). DUNE offers complementary but weaker coverage due to its lower beam energy (120 GeV vs. 400 GeV), reaching  $f \sim \text{few} \times 10^8$  GeV at  $m_J \simeq 1$  GeV. At the LHC, MATHUSLA’s large off-axis geometric acceptance compensates for the transverse production kinematics of the majorons from  $\tau$  decays, yielding reach comparable to DUNE and exceeding that of FASER2 and FPF FASER2, which are optimized for the highly forward regime. The full ordering of experiments by maximum reach in  $f$  (for the anarchical benchmarks) is: SHiP, DUNE, MATHUSLA, FPF FASER2, NA62, and FASER2.

At lepton colliders running on the  $Z$  pole (FCC-ee), the leading majoron production mode is  $Z \rightarrow J\gamma$  via the  $g_{JZ\gamma}$  coupling (Eq. (4.4)). Even with  $N_Z = 2.5 \times 10^{12}$   $Z$  bosons, the resulting reach ( $1/f \sim 10^{-3}$ – $10^{-2}$  GeV $^{-1}$  for the background-free channel  $J \rightarrow \gamma\gamma$ , and  $10^{-4}$ – $10^{-3}$  GeV $^{-1}$  for leptonic decays) is not competitive with beam dump experiments; we therefore omit FCC-ee from the sensitivity figures. At the LHC, Drell-Yan, vector-boson fusion, and sterile-neutrino-mediated production channels lead to limits that are similarly non-competitive with dedicated FV searches and astrophysical bounds [51].

**Benchmark dependence:** The qualitative sensitivity pattern is similar within each class of  $K$ -matrix benchmarks, since in all cases  $J$  is produced predominantly via a single process ( $\tau$  decays). Nevertheless, the detailed reach of a given experiment can vary by up to an order of magnitude in  $1/f$  across benchmarks, reflecting the exponential sensitivity of the displaced-decay probability (Eq. (4.1)) to the majoron lifetime and the quadratic dependence of the number of displaced decays on the off-diagonal entries of the  $K$  matrix.

The opposite trends visible in Fig. 4 compared to Figs. 5–6 have a simple origin in parameterization. In the anarchical ansatz (Eq. (2.14)), the off-diagonal couplings governing  $\tau \rightarrow \ell J$  production are fixed to unity; increasing  $R_J$  thus only shortens the majoron lifetime (via enhanced diagonal decay couplings), shifting the sensitivity contour to smaller  $1/f$ . Conversely, for the single-flavor textures (Eq. (2.17)) and CP-violating benchmarks (Eq. (2.19)), the diagonal entries are fixed and the off-diagonal coupling  $\kappa$  is varied. Increasing  $\kappa$  simultaneously enhances the production rate ( $\propto \kappa^2$ ) and shortens the lifetime ( $\propto 1/\kappa^2$ ); however, since for most of the parameter space the experiments operate in the long-lifetime regime ( $\gamma\beta c\tau \gg L_{\max}$ ), the production-rate gain dominates, and the net sensitivity improves substantially with increasing  $\kappa$ .

We note that the benchmark  $R_J = 2/3$ , employed in Ref. [31], yields a  $K$  matrix that is not positive semi-definite (cf. discussion below Eq. (2.14)) and therefore lies outside the physical parameter space of the minimal singlet majoron model. We retain it for comparison, but emphasize that only the  $R_J = 1.01$  and  $R_J = 10$  benchmarks are physical—using the Casas–Ibarra parametrization [72], the former can be viewed as approaching the regime of near-maximal mixing among the diagonal and off-diagonal entries of  $K$  [31], while the latter corresponds to either a larger number of sterile neutrinos or to a small negative value of  $K^o$ .

**Complementary constraints:** In Figs. 4–6, we overlay existing constraints and projections from several independent probes, both terrestrial LFV searches and astrophysical

bounds. Since such limits have been thoroughly discussed in a recent study of an axially-coupled ALP, Ref. [37], we follow their discussion and use the digitized data in the GitHub repository accompanying [37] to recast the limits from axially-coupled ALP into majoron.

Supernova bounds: using the cooling bound, we recast the bounds separately from flavor-conserving couplings (SN- $ee$  and SN- $\mu\mu$ , from Refs. [37, 68]) and from flavor-violating couplings (SN- $e\mu$ , from Ref. [20]). These astrophysical bounds provide the strongest existing limits for  $m_J \lesssim 200$  MeV, but lose sensitivity once  $m_J$  exceeds the proto-neutron-star core temperature,  $T_{\text{core}} \sim 30\text{--}50$  MeV.

LFV searches: we recast the limits from  $\mu \rightarrow e + J_{\text{inv}}$ . [73–76],  $\mu \rightarrow e + \gamma$  [77],  $\tau$  lifetime [78],  $\tau \rightarrow \mu + J_{\text{inv}}$ . [79–81],  $\tau \rightarrow \mu + J_{\text{vis}}$ . [82–87]. Where applicable, we also display projected sensitivities from Belle II [68, 88] and MEG-II [89].

**Gap-filling role of intensity-frontier searches:** The sensitivity projections presented here demonstrate that beam dump and forward-physics experiments fill a critical gap in the intermediate mass window  $200 \text{ MeV} \lesssim m_J \lesssim 1 \text{ GeV}$ , between supernova cooling bounds that lose sensitivity at  $m_J \gtrsim T_{\text{core}}$  and  $B$ -factory or dedicated LFV searches that provide coverage primarily above  $\sim 1$  GeV. These experiments thus emerge as the leading terrestrial probes of the seesaw parameter space in this mass range.

## 6 Conclusions

We have performed a comprehensive study of the sensitivity of current and future IF experiments to a sub-GeV singlet majoron—the pseudo-Nambu–Goldstone boson of spontaneously broken  $U(1)_{B-L}$  in the type-I seesaw framework. Unlike a generic ALP with FV couplings, the majoron’s coupling structure is entirely determined by the seesaw parameters, making each experimental measurement a direct probe of the neutrino mass generation mechanism.

The key finding of this work is that LFV  $\tau$  decays,  $\tau \rightarrow \mu J$  and  $\tau \rightarrow e J$ , provide the dominant majoron production mechanism in proton beam dump experiments and LHC forward detectors, opening the mass window  $200 \text{ MeV} \lesssim m_J \lesssim m_\tau - m_e$  to experimental scrutiny. As demonstrated in Sec. 5, this LFV-driven production, combined with the background-free displaced decay signatures into charged leptons (with the same or different flavors), allows intensity-frontier searches to fill the gap between supernova cooling bounds (which lose sensitivity for  $m_J \gtrsim T_{\text{core}}$ ) and  $B$ -factory or dedicated LFV searches at higher majoron masses. Among the experiments considered, SHiP offers the highest projected reach ( $f$  up to  $\sim 10^9$  GeV), followed by DUNE, MATHUSLA, FPF FASER2, NA62, and FASER2, while collider searches at the LHC and FCC-ee are not competitive in this parameter region.

Our analysis is complementary to recent studies of FV ALPs. In particular, Ref. [31] employed the benchmark  $R_J = 2/3$ , which we have shown lies outside the physical parameter space of the minimal singlet majoron model (the  $K$  matrix is not positive semi-definite), motivating the alternative benchmarks introduced in this work. Ref. [37] investigated a purely axially-coupled ALP whose coupling structure—in particular, the relation between

vector and axial couplings—does not directly map onto the singlet majoron. We have studied a broad class of physically motivated  $K$ -matrix textures: anarchical (Eq. (2.14)), single-flavor (Eq. (2.17)), and CP-violating parameterizations motivated by leptogenesis (Eq. (2.19)). While the qualitative picture is robust across benchmarks—LFV  $\tau$  decays dominate production, and leptonic final states dominate the visible decay—the quantitative reach varies by up to an order of magnitude in the  $U(1)_{B-L}$  breaking scale  $f$ , reflecting the exponential sensitivity to the majoron lifetime and hierarchy between off-diagonal and diagonal entries of the  $K$  matrix.

Looking ahead, several experimental developments will provide important complementary coverage. Belle II [88], with its large  $\tau$ -pair samples, will directly constrain the LFV branching fraction  $\text{BR}(\tau \rightarrow \ell J)$  that drives majoron production in our analysis. Moreover, MEG-II [89] will improve limits on  $\mu \rightarrow e J$ , probing the off-diagonal  $K_{e\mu}$  entry with unprecedented precision. The proposed Super Tau-Charm Facility [38, 90] could extend the reach further via high-statistics  $\tau$  production. On the theoretical side, improved modeling of forward charm production—the dominant systematic uncertainty in our projections—will sharpen the sensitivity forecasts. Together with the beam dump and forward-detector searches studied here, these efforts will comprehensively test the singlet majoron across the sub-GeV mass range, directly probing the structure of the seesaw mechanism at IF facilities.

## Acknowledgments

The authors gratefully acknowledge the valuable discussions and insights provided by the members of the China Collaboration of Precision Testing and New Physics. KJ and CTL are supported by the National Natural Science Foundation of China (NNSFC) under grants No. 12335005, No. 12575118, and the Special funds for postdoctoral overseas recruitment, Ministry of Education of China.

## References

- [1] P. Minkowski, “ $\mu \rightarrow e\gamma$  at a rate of one out of  $10^9$  muon decays?,” *Physics Letters B* **67** (1977) 421–428.
- [2] M. Gell-Mann, P. Ramond, and R. Slansky, “Complex spinors and unified theories,” in *Supergravity*, P. V. Nieuwenhuizen and D. Freedman, eds. 1979. Proceedings of the Stony Brook workshop; seminal seesaw discussion.
- [3] T. Yanagida, “Horizontal symmetry and masses of neutrinos,” in *Proceedings of the Workshop on the Unified Theory and the Baryon Number in the Universe*. 1979. KEK, Tsukuba proceedings.
- [4] R. N. Mohapatra and G. Senjanović, “Neutrino mass and spontaneous parity nonconservation,” *Physical Review Letters* **44** (1980) 912–915.
- [5] Y. Chikashige, R. N. Mohapatra, and R. D. Peccei, “Are There Real Goldstone Bosons Associated with Broken Lepton Number?,” *Phys. Lett. B* **98** (1981) 265–268.

- [6] G. Gelmini and M. Roncadelli, “Left-handed neutrino mass scale and spontaneously broken lepton number,” *Phys. Lett. B* **99** (1981) 411–415.
- [7] J. Schechter and J. W. F. Valle, “Neutrino Decay and Spontaneous Violation of Lepton Number,” *Phys. Rev. D* **25** (1982) 774.
- [8] S. B. Giddings and A. Strominger, “Baby Universes, Third Quantization and the Cosmological Constant,” *Nucl. Phys. B* **321** (1989) 481–508.
- [9] D. Harlow and H. Ooguri, “Symmetries in Quantum Field Theory and Quantum Gravity,” *Commun. Math. Phys.* **376** no. 3, (2020) 1779–1845.
- [10] D. Harlow and H. Ooguri, “Constraints on Symmetries from Holography,” *Phys. Rev. Lett.* **122** no. 19, (2019) 191601.
- [11] S. B. Giddings and A. Strominger, “Axions and the Cosmological Constant,” *Nucl. Phys. B* **306** (1988) 890–907.
- [12] S. R. Coleman, “Black Holes as Red Herrings: Topological Fluctuations and the Loss of Quantum Coherence,” *Nucl. Phys. B* **307** (1988) 867–882.
- [13] L. Abbott and M. B. Wise, “Wormholes and Global Symmetries,” *Nucl. Phys. B* **325** (1989) 687–704.
- [14] S. Chang, S. Ganguly, T. Jung, T.-S. Park, and C. Shin, “Constraining meV to 10 gev majoron by big bang nucleosynthesis,” *Phys. Rev. D* **110** (2024) 015019.
- [15] C. García-Cely, A. Ibarra, *et al.*, “Neutrino lines from majoron dark matter,” *JHEP* (2017) .
- [16] S. Chang, S. Ganguly, T. H. Jung, T.-S. Park, and C. S. Shin, “Constraining MeV to 10 GeV Majorons by big bang nucleosynthesis,” *Phys. Rev. D* **110** no. 1, (2024) 015019, [arXiv:2401.00687 \[hep-ph\]](#).
- [17] K. Choi, C. W. Kim, J. Kim, and W. P. Lam, “Constraints on the Majoron Interactions From the Supernova SN1987A,” *Phys. Rev. D* **37** (1988) 3225.
- [18] D. F. G. Fiorillo, G. G. Raffelt, and E. Vitagliano, “Strong supernova 1987a constraints on bosons decaying to neutrinos,” *Physical Review Letters* **131** no. 2, (2023) 021001.
- [19] K. Akita, S. H. Im, M. Masud, and S. Yun, “Limits on heavy neutral leptons,  $Z'$  bosons and majorons from high-energy supernova neutrinos,” *JHEP* **07** (2024) 057.
- [20] Y. Li and Z. Liu, “Supernova constraints on lepton flavor violating ALPs,” [arXiv:2501.12075 \[hep-ph\]](#).
- [21] Z.-M. Huang and Z. Liu, “Low-energy supernova constraints on lepton flavor violating axions,” *JHEP* **10** (2025) 024, [arXiv:2506.16922 \[hep-ph\]](#).
- [22] Z.-M. Huang, C. Li, and Z. Liu, “Refined Low-Energy Supernova Constraints on Lepton Flavor Violating Axions,” [arXiv:2510.22523 \[hep-ph\]](#).
- [23] J. Heck and H. Patel, “The majoron at two loops,” *Phys. Rev. D* **100** (2019) 095015.
- [24] E. Bertuzzo, A. L. Foguel, G. M. Salla, and R. Zukanovich Funchal, “New limits on leptophilic axionlike particles and majorons from argoneut,” *Physical Review Letters* **130** (2023) 171801.
- [25] Y. Cheng, C.-W. Chiang, X.-G. He, and J. Sun, “Flavor-changing Majoron interactions with leptons,” *Phys. Rev. D* **104** no. 1, (2021) 013001, [arXiv:2012.15287 \[hep-ph\]](#).

- [26] P. Escribano, M. Hirsch, J. Nava, and A. Vicente, “Observable flavor violation from spontaneous lepton number breaking,” *JHEP* **01** (2022) 098, [arXiv:2108.01101 \[hep-ph\]](#).
- [27] A. Herrero-Brocal and A. Vicente, “The majoron coupling to charged leptons,” *JHEP* **01** (2024) 078, [arXiv:2311.10145 \[hep-ph\]](#).
- [28] J. Heeck and W. Rodejohann, “Lepton Flavor Violation with Displaced Vertices,” *Phys. Lett.* **B776** (2018) 385–390.
- [29] A. Herrero-Brocal, “Non-anomalous axions: lessons from the Majoron,” [arXiv:2602.22311 \[hep-ph\]](#).
- [30] J. Quevillon and C. Smith, “Axions are blind to anomalies,” *Eur. Phys. J. C* **79** no. 10, (2019) 822.
- [31] E. Bertuzzo, A. L. Foguel, G. M. Salla, and R. Z. Funchal, “New Limits on Leptophilic Axionlike Particles and Majorons from ArgoNeUT,” *Phys. Rev. Lett.* **130** no. 17, (2023) 171801.
- [32] J. Heeck and H. H. Patel, “Majoron at two loops,” *Phys. Rev. D* **100** no. 9, (2019) 095015.
- [33] A. Pilaftsis, “Astrophysical and terrestrial constraints on singlet Majoron models,” *Phys. Rev. D* **49** (1994) 2398–2404.
- [34] A. Broncano, M. B. Gavela, and E. E. Jenkins, “The Effective Lagrangian for the seesaw model of neutrino mass and leptogenesis,” *Phys. Lett. B* **552** (2003) 177–184. [Erratum: *Phys.Lett.B* 636, 332 (2006)].
- [35] S. Davidson, G. Isidori, and A. Strumia, “The smallest neutrino mass,” *Phys. Lett.* **B646** (2007) 100–104.
- [36] W. Altmannshofer, J. A. Dror, and S. Gori, “New Opportunities for Detecting Axion-Lepton Interactions,” *Phys. Rev. Lett.* **130** no. 24, (2023) 241801.
- [37] Y. Ema, P. J. Fox, M. Hostert, T. Menzo, M. Pospelov, A. Ray, and J. Zupan, “Long-lived axionlike particles from tau decays,” *Phys. Rev. D* **112** no. 11, (2025) 115028.
- [38] X.-H. Jiang and C.-T. Lu, “Searching for axion-like particles from tau exotic decays at the Super Tau-Charm Facility and its far detectors,” [arXiv:2509.23949 \[hep-ph\]](#).
- [39] Y. Aoki *et al.*, “FLAG Review 2024,”.
- [40] C. Alexandrou, S. Bacchio, J. Finkenrath, C. Iona, G. Koutsou, Y. Li, and G. Spanoudes, “Nucleon charges and  $\sigma$ -terms in lattice QCD,” *Phys. Rev. D* **111** no. 5, (2025) 054505.
- [41] T. Sjöstrand, S. Ask, J. R. Christiansen, R. Corke, N. Desai, P. Ilten, S. Mrenna, S. Prestel, C. O. Rasmussen, and P. Z. Skands, “An introduction to PYTHIA 8.2,” *Comput. Phys. Commun.* **191** (2015) 159–177.
- [42] P. Skands, S. Carrazza, and J. Rojo, “Tuning PYTHIA 8.1: the Monash 2013 Tune,” *Eur. Phys. J. C* **74** no. 8, (2014) 3024.
- [43] E.-J. Ahn, R. Engel, T. K. Gaisser, P. Lipari, and T. Stanev, “Cosmic ray interaction event generator SIBYLL 2.1,” *Phys. Rev. D* **80** (2009) 094003, [arXiv:0906.4113 \[hep-ph\]](#).
- [44] J. Alda, M. Fuentes Zamoro, L. Merlo, X. Ponce Díaz, and S. Rigolin, “ALPaca: The ALP Automatic Computing Algorithm,”.
- [45] D. Aloni, Y. Soreq, and M. Williams, “Coupling QCD-Scale Axionlike Particles to Gluons,” *Phys. Rev. Lett.* **123** no. 3, (2019) 031803.

- [46] M. Bauer, M. Neubert, and A. Thamm, “Collider Probes of Axion-Like Particles,” *JHEP* **12** (2017) 044.
- [47] M. A. Shifman, “Quark hadron duality,” in *8th International Symposium on Heavy Flavor Physics*, vol. 3, pp. 1447–1494. World Scientific, Singapore, 7, 2000.
- [48] S.-Y. Wang, Y.-P. Jiao, H.-H. Zhang, and G. Cacciapaglia, “Probing Long-Lived Photophobic Axion-Like Particles via Prompt Leptons and Mono- $\gamma$  at FCC-ee and CEPC,”.
- [49] J. Alimena *et al.*, “Searching for long-lived particles beyond the Standard Model at the Large Hadron Collider,” *J. Phys. G* **47** no. 9, (2020) 090501, [arXiv:1903.04497 \[hep-ex\]](#).
- [50] D. d’Enterria and V. D. Le, “Rare and exclusive few-body decays of the Higgs, Z, W bosons, and the top quark,” *J. Phys. G* **52** no. 5, (2025) 053001, [arXiv:2312.11211 \[hep-ph\]](#).
- [51] C. Bustos, G. Ardila, and W. Rodejohann, “Neutrino masses and majoron production in the type 1 seesaw mechanism.” <https://indico.global/event/8704/contributions/83880>, December, 2022.
- [52] L. A. Anchordoqui *et al.*, “The Forward Physics Facility: Sites, experiments, and physics potential,” *Phys. Rept.* **968** (2022) 1–50.
- [53] C. Anderson *et al.*, “The ArgoNeuT Detector in the NuMI Low-Energy beam line at Fermilab,” *JINST* **7** (2012) P10019.
- [54] A. M. Cooper-Sarkar *et al.*, “Search for Heavy Neutrino Decays in the BEBC Beam Dump Experiment,” *Phys. Lett. B* **160** (1985) 207–211.
- [55] R. Barouki, G. Marocco, and S. Sarkar, “Blast from the past II: Constraints on heavy neutral leptons from the BEBC WA66 beam dump experiment,” *SciPost Phys.* **13** (2022) 118.
- [56] F. Bergsma *et al.*, “Search for Axion Like Particle Production in 400-GeV Proton - Copper Interactions,” *Phys. Lett. B* **157** (1985) 458–462.
- [57] B. Döbrich, J. Jaeckel, and T. Spadaro, “Light in the beam dump - ALP production from decay photons in proton beam-dumps,” *JHEP* **05** (2019) 213. [Erratum: *JHEP* 10, 046 (2020)].
- [58] V. Hewes *et al.*, “Deep Underground Neutrino Experiment (DUNE) Near Detector Conceptual Design Report,” *Instruments* **5** no. 4, (2021) 31.
- [59] L. A. Anchordoqui *et al.*, “The Forward Physics Facility at the Large Hadron Collider,” 3, 2025.
- [60] J. L. Feng, I. Galon, F. Kling, and S. Trojanowski, “Axionlike particles at FASER: The LHC as a photon beam dump,” *Phys. Rev. D* **98** no. 5, (2018) 055021.
- [61] J. L. Feng *et al.*, “The Forward Physics Facility at the High-Luminosity LHC,”.
- [62] K. Jodłowski and S. Trojanowski, “Neutrino beam-dump experiment with FASER at the LHC,” *JHEP* **05** (2021) 191.
- [63] B. Aitken *et al.*, “MATHUSLA: An External Long-Lived Particle Detector to Maximize the Discovery Potential of the HL-LHC,”.
- [64] K. Jodłowski, F. Kling, L. Roszkowski, and S. Trojanowski, “Extending the reach of FASER, MATHUSLA, and SHiP towards smaller lifetimes using secondary particle production,” *Phys. Rev. D* **101** no. 9, (2020) 095020.

- [65] J. Blümlein and J. Brunner, “New Exclusion Limits on Dark Gauge Forces from Proton Bremsstrahlung in Beam-Dump Data,” *Phys. Lett. B* **731** (2014) 320–326.
- [66] **FASER** Collaboration, H. Abreu *et al.*, “First neutrino interaction candidates at the LHC,” *Phys. Rev. D* **104** no. 9, (2021) L091101, [arXiv:2105.06197 \[hep-ex\]](#).
- [67] A. Ariga, R. Balkin, I. Galon, E. Kajomovitz, and Y. Soreq, “Hunting muonic forces at emulsion detectors,” *Phys. Rev. D* **109** no. 3, (2024) 035003, [arXiv:2305.03102 \[hep-ph\]](#).
- [68] L. Calibbi, D. Redigolo, R. Ziegler, and J. Zupan, “Looking forward to lepton-flavor-violating ALPs,” *JHEP* **09** (2021) 173.
- [69] J. Blumlein *et al.*, “Limits on neutral light scalar and pseudoscalar particles in a proton beam dump experiment,” *Z. Phys. C* **51** (1991) 341–350.
- [70] **NA62** Collaboration, E. Cortina Gil *et al.*, “The Beam and detector of the NA62 experiment at CERN,” *JINST* **12** no. 05, (2017) P05025, [arXiv:1703.08501 \[physics.ins-det\]](#).
- [71] **FASER** Collaboration, A. Ariga *et al.*, “FASER’s physics reach for long-lived particles,” *Phys. Rev. D* **99** no. 9, (2019) 095011, [arXiv:1811.12522 \[hep-ph\]](#).
- [72] J. A. Casas and A. Ibarra, “Oscillating neutrinos and  $\mu \rightarrow e, \gamma$ ,” *Nucl. Phys. B* **618** (2001) 171–204, [arXiv:hep-ph/0103065](#).
- [73] **TWIST** Collaboration, R. Bayes *et al.*, “Search for two body muon decay signals,” *Phys. Rev. D* **91** no. 5, (2015) 052020, [arXiv:1409.0638 \[hep-ex\]](#).
- [74] **PIENU** Collaboration, A. Aguilar-Arevalo *et al.*, “Improved search for two body muon decay  $\mu^+ \rightarrow e^+ X_H$ ,” *Phys. Rev. D* **101** no. 5, (2020) 052014, [arXiv:2002.09170 \[hep-ex\]](#).
- [75] S. E. Derenzo, “Measurement of the low-energy end of the mu-plus decay spectrum,” *Phys. Rev.* **181** (1969) 1854–1866.
- [76] R. Bilger, K. Foehl, H. Clement, M. Croni, A. Erhardt, R. Meier, J. Patzold, and G. J. Wagner, “Search for exotic muon decays,” *Phys. Lett. B* **446** (1999) 363–367, [arXiv:hep-ph/9811333](#).
- [77] M. Bauer, M. Neubert, S. Renner, M. Schnubel, and A. Thamm, “Flavor probes of axion-like particles,” *JHEP* **09** (2022) 056, [arXiv:2110.10698 \[hep-ph\]](#).
- [78] **Particle Data Group** Collaboration, S. Navas *et al.*, “Review of particle physics,” *Phys. Rev. D* **110** no. 3, (2024) 030001.
- [79] **ARGUS** Collaboration, H. Albrecht *et al.*, “A Search for lepton flavor violating decays tau  $\rightarrow e$  alpha, tau  $\rightarrow \mu$  alpha,” *Z. Phys. C* **68** (1995) 25–28.
- [80] **Belle** Collaboration, K. Uno *et al.*, “Search for lepton-flavor-violating tau decays to  $\ell\alpha$  at Belle,” *JHEP* **08** (2025) 155, [arXiv:2503.22195 \[hep-ex\]](#).
- [81] **Belle-II** Collaboration, I. Adachi *et al.*, “Search for Lepton-Flavor-Violating  $\tau$  Decays to a Lepton and an Invisible Boson at Belle II,” *Phys. Rev. Lett.* **130** no. 18, (2023) 181803, [arXiv:2212.03634 \[hep-ex\]](#).
- [82] **BaBar** Collaboration, J. P. Lees *et al.*, “Limits on tau Lepton-Flavor Violating Decays in three charged leptons,” *Phys. Rev. D* **81** (2010) 111101, [arXiv:1002.4550 \[hep-ex\]](#).
- [83] K. Hayasaka *et al.*, “Search for Lepton Flavor Violating Tau Decays into Three Leptons with 719 Million Produced Tau+Tau- Pairs,” *Phys. Lett. B* **687** (2010) 139–143, [arXiv:1001.3221 \[hep-ex\]](#).

- [84] **ATLAS** Collaboration, G. Aad *et al.*, “Probing lepton flavour violation via neutrinoless  $\tau \rightarrow 3\mu$  decays with the ATLAS detector,” *Eur. Phys. J. C* **76** no. 5, (2016) 232, [arXiv:1601.03567 \[hep-ex\]](#).
- [85] **CMS** Collaboration, A. M. Sirunyan *et al.*, “Search for the lepton flavor violating decay  $\tau \rightarrow 3\mu$  in proton-proton collisions at  $\sqrt{s} = 13$  TeV,” *JHEP* **01** (2021) 163, [arXiv:2007.05658 \[hep-ex\]](#).
- [86] **LHCb** Collaboration, R. Aaij *et al.*, “Search for the lepton flavour violating decay  $\tau^- \rightarrow \mu^- \mu^+ \mu^-$ ,” *JHEP* **02** (2015) 121, [arXiv:1409.8548 \[hep-ex\]](#).
- [87] **Belle-II** Collaboration, I. Adachi *et al.*, “Search for lepton-flavor-violating  $\tau^- \rightarrow \mu^- \mu^+ \mu^-$  decays at Belle II,” *JHEP* **09** (2024) 062, [arXiv:2405.07386 \[hep-ex\]](#).
- [88] **Belle-II** Collaboration, D. Rodríguez Pérez, “Prospects for  $\tau$  Lepton Physics at Belle II,” in *17th Conference on Flavor Physics and CP Violation*. 6, 2019. [arXiv:1906.08950 \[hep-ex\]](#).
- [89] **MEG II** Collaboration, A. M. Baldini *et al.*, “The design of the MEG II experiment,” *Eur. Phys. J. C* **78** no. 5, (2018) 380, [arXiv:1801.04688 \[physics.ins-det\]](#).
- [90] X.-C. Ai *et al.*, “Conceptual design report of the Super Tau-Charm Facility: the accelerator,” *Nucl. Sci. Tech.* **36** no. 12, (2025) 242, [arXiv:2509.11522 \[physics.acc-ph\]](#).